International Journal of Multiphase Flow 144 (2021) 103778

Contents lists available at ScienceDirect

International Journal of Multiphase Flow

journal homepage: www.elsevier.com/locate/ijmulflow

Stochastic mechanistic modelling of two-phase slug flow forces on bends in horizontal piping

Arnout M. Klinkenberg *, Arris S. Tijsseling

Aker Solutions ASA, P.O. Box 169, 1325 Lysaker, Norway
Department of Mathematics and Computer Science, Eindhoven University of Technology, P.O. Box 513, 5600 MB Eindhoven, The Netherlands

ARTICLE INFO

Keywords:
Pipe
Vibration
Two-phase
Slug
Force
Bend
Elbow

ABSTRACT

Slug flow through piping systems may cause severe mechanical vibrations. Finite element models, commonly used to predict dynamic pipe stresses and fatigue, require the slug excitation force as boundary condition.

In this paper, a stochastic mechanistic model of the slug force acting on a pipe bend is proposed. The force induced by continuous hydrodynamic two-phase slug flow is modelled by the momentum balance over the bend using slug quantities as liquid holdup and phase velocity. The two-phase flow is described by a train of slug units. Each unit is divided into a film zone with a constant liquid height and a slug zone with aerated liquid. Two-phase flows have a stochastic character, but models based on a fixed slug length cannot predict stochastic force variations. A new approach is introduced that includes the stochastic character of slug flow in the force calculations. A unit slug model is adapted with a log-normal distribution as closure for the slug zone length, resulting in an improved model with stochastic properties. A Lagrangian approach is used to solve the governing equations.

Results of the new model are compared with bend force measurements found in the literature. Most of the published measurements were done with air and water under atmospheric conditions. In many field applications, the fluids and operational conditions are different from those used in laboratory experiments. The stochastic mechanistic approach, where the main equations are based on physical laws, increases the models applicability outside the atmospheric air and water conditions used for the validation.

1. Introduction

Multiple phases are often simultaneously transported through pipelines. Heat recovery installations in power plants are producing steam by heating water flowing in tubes inside the exhaust gas ducts. The steam is used to generate electricity by driving a steam engine or for other processes in the plant. Due to the evaporation of the water, a two-phase flow exists in the tubing. A similar process is used for the cooling of nuclear power reactors, where the liquids used to cool the reactor core are evaporating. Multiphase flow is common for oil and gas production where gas, oil, and water are transported through the production piping.

Depending on the volumetric flow rates of the different phases, the pipe diameter, and the fluid properties, different flow patterns can exist in gas–liquid pipe flow. Slug flow is a frequently observed flow pattern where aerated liquid pockets (the slug zone) and large gas bubbles (the film zone) are alternating in the pipeline. The irregular gas and liquid fractions in the pipe cause velocity, pressure, and density fluctuations, which are inducing fluctuating forces on bends and other flow-turning or flow-resisting elements.

Unsteady forces on the pipe bends will result in pipe vibrations and an elevated risk of fatigue failure. Whether the vibrations will result in severe damage depends on the design of the piping system and the frequency spectrum of the slug-train force. Finite element methods are generally used (Pontaza and Menon, 2011; Urthaler et al., 2011; Pontaza et al., 2017) to evaluate the design of the piping system by simulating the stress response to fluid forces. The required fluid excitation forces can be calculated by Computational Fluid Dynamics (CFD) (Mack et al., 2018; Pontaza, 2014; Hossain et al., 2019) or scaling rules can be used to reconstruct the force spectrum (Giraudeau et al., 2013; Belfroid et al., 2018).

A new, alternative method is developed herein to predict the excitation force of slugs flowing through a pipe bend. The results are compared with measured data found in the literature. The model is based on the momentum balance over the pipe bend when slugs and

* Corresponding author at: Department of Mathematics and Computer Science, Eindhoven University of Technology, P.O. Box 513, 5600 MB Eindhoven, The Netherlands.
E-mail address: arnout.klinkenberg@gmail.com (A.M. Klinkenberg).

https://doi.org/10.1016/j.ijmultiphaseflow.2021.103778
Received 6 January 2021; Received in revised form 14 June 2021; Accepted 4 August 2021
Available online 10 August 2021

bubbles are flowing through it. The liquid holdup, defined as the fraction of the pipe cross-section occupied by liquid, and the different phase velocities within the unit slug are described by a one-dimensional *unit slug* model satisfying the conservation of mass and momentum for both zones. Empirical sub-models are required to complete the system of equations. Conventionally, the unit slug model assumes a fixed slug zone length and therefore cannot predict the observed stochastic flow variations (Taitel and Barnea, 1990; Gomez et al., 2000a). To model the missing stochastic character, the fixed slug zone length has been replaced by a probabilistically distributed length. The proposed adaption results in an improved slug model with stochastic slug lengths. The corresponding film lengths are calculated from a mass balance.

The model solution requires neither spatial discretization nor a lengthy iterative solver, which hugely shortens the calculation times compared to CFD calculations. Depending on the high-performance computer systems used for the latter, the expected speed-up of the mechanistic model using one processor is a factor 10^4 to 10^6. However, the introduced simplification will cause errors in the slug flow properties. The comparison with measured data will reveal whether a unit slug model with a stochastic slug length closure can be used to reliably calculate forces on pipe bends.

1.1. Previous studies

Several approaches to calculate the frequency spectrum of the fluid forces can be found in the literature. Yih and Griffith (1968) proposed a method based on their force measurements of two-phase flow in a vertical pipe, hitting a horizontal plate when flowing out of the pipe. Using correlations for the Root Mean Square (RMS) value of the force, two constants describing the (log–log) triangular shape of the spectrum, and the peak frequency, the measured Power Spectral Density (PSD) could be reconstructed for the given volumetric flow rates and fluid properties. Riverin et al. (2006), Riverin and Pettigrew (2007) and Giraudeau et al. (2011, 2013) adopted the frequency-domain approach of Yih and Griffith (1968). Different pipe diameters and bend radii were used in the upward two-phase flow force measurements. Similar to Yih and Griffith, the scaling rule to estimate the RMS value was based on the Weber number We:

$$We = \frac{\rho_l u_m^2 D}{\sigma} \tag{1}$$

where D is the pipe inner diameter, ρ_l the liquid density and σ the surface tension. For artificial velocities, the symbol u is used. The mixture or average velocity u_m is defined as the sum of the superficial gas and liquid velocities u_g and u_l, i.e. the upstream injected gas and liquid volume flows divided by the pipe cross section. The RMS force is:

$$F_{rms} = C \rho_l u_m^2 A\, We^{-0.4} \tag{2}$$

where A is the cross section of the pipe and C is an empirical constant. Both $C = 10$ and $C = 25$ have been proposed to fit the measurements. Nennie et al. (2013) used slug tracking and a zone-specific density to predict slug forces on bends. A stochastic time dependency was introduced by a normally distributed slug frequency. Pressure fluctuations were included in the model, but details were not disclosed. Belfroid et al. (2018) extended the RMS formula (2) with a dependency on liquid volume fraction $\lambda_l = u_l/u_m$:

$$F_{rms} = C \rho_l u_m^2 A\, We^{-0.4} \begin{cases} 5\lambda_l, & \text{if } 0.01 < \lambda_l < 0.2 \\ 1, & \text{if } 0.2 \le \lambda_l \le 0.8 \\ 5\left(1-\lambda_l\right), & \text{if } 0.8 < \lambda_l < 0.99\,. \end{cases} \tag{3}$$

Belfroid et al. (2018) suggested a value for C in Eq. (3) depending on the bend radius: $C = 24$ for a bend with a $1.5D$ radius and $C = 30$ for one with a $3.0D$ radius. The formula is based on force measurements on horizontal pipe bends with different pipe diameters and bend radii (Belfroid et al., 2010; Nennie et al., 2013; Belfroid et al., 2018), extended with published bend force data by Giraudeau et al. (2013), Tay and Thorpe (2014, 2017) and Liu et al. (2012). Its dependency on gas and liquid surface tension σ is questionable, as the empirical formula is based on air and water measurements only. Both the measurements done by Zukoski (1966) of the Taylor bubble velocity and the measurements done by Tay and Thorpe (2004) of slug force on a bend showed not more than a minor effect of surface tension. Since all measurements were performed under nearly atmospheric conditions, where the gas density is low compared with the liquid density, the model does not include the gas density so that any effect of high pressure on the bend force is not included.

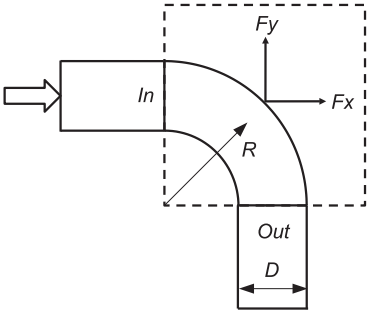

Fig. 1. Control volume around the pipe bend.

Tay and Thorpe (2004, 2014, 2017) published the *Piston Flow Model* (PFM), a time-domain approach to estimate the forces on pipe bends. The slug flow was modelled as a train of alternating pure liquid *pistons* and pure gas pockets with constant lengths, equal to the measured average slug and bubble lengths. The bend force was calculated with a momentum balance:

$$\mathbf{F}_{bend} = \int_{CS} p\,\mathbf{n}\,dA - \int_{CS} \mathbf{v}\rho(\mathbf{v}\cdot\mathbf{n})\,dA - \frac{d}{dt}\int_{CV} \mathbf{v}\rho dV\,. \tag{4}$$

where CV is the control volume as shown in Fig. 1 and CS is the control surface. Density ρ, pressure p and velocity $\mathbf{v}$ are time depending quantities. In Tay's approach, both gas and liquid pockets were flowing with the translational gas–liquid interface velocity v_T (Nicklin et al., 1962a):

$$v_T = 1.2u_m + v_{drift}\,. \tag{5}$$

For the drift velocity v_{drift}, a closure formula depending on surface tension was proposed by Tay and Thorpe (2014). Since a constant translational velocity v_T was assumed, the predicted force fluctuations are only caused by density and pressure variations in the control volume. Tay and Thorpe (2014) determined the pressure at the control volume boundaries by calculating the frictional loss of the liquid and gas pockets in between the bend and the outlet, assuming a fixed pressure at the outflow. For all tested flow conditions, a good match was found between the measured and predicted peak forces. Despite the good results, the validity of the model is questionable. The assumption that both slug and bubble travel at the translational velocity v_T, which is more than 1.2 times the average velocity u_m (Eq. (5)), violates the conservation of fluid mass and momentum. Since average slug and film lengths were used, the bend-force time-signal is periodic and the power spectrum is, contrary to observations, not continuous but discrete. Furthermore, using measured slug and film lengths as input into a model limits its practical use.

Liu et al. (2012) measured two-phase flow forces on a vertical to horizontal bend. A strong correlation between the liquid holdup and the force fluctuations was observed. Based on a force balance over a bend, the same equations as Tay and Thorpe (2014) were found, except for a new term that included a local impact force. Besides a comprehensive review, Miwa et al. (2015) modelled the additional term introduced by Liu et al. (2012) by considered possible water hammer effects (pressure

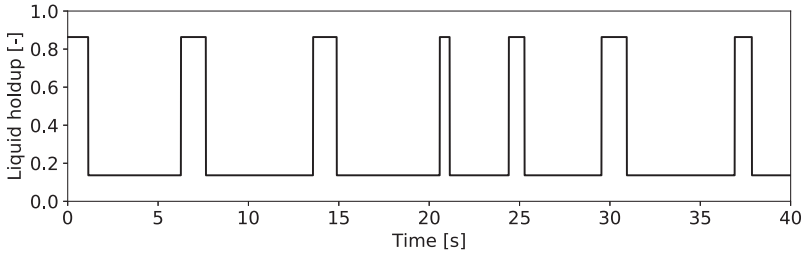

Fig. 2. Two discrete levels of liquid holdup in the mechanistic model.

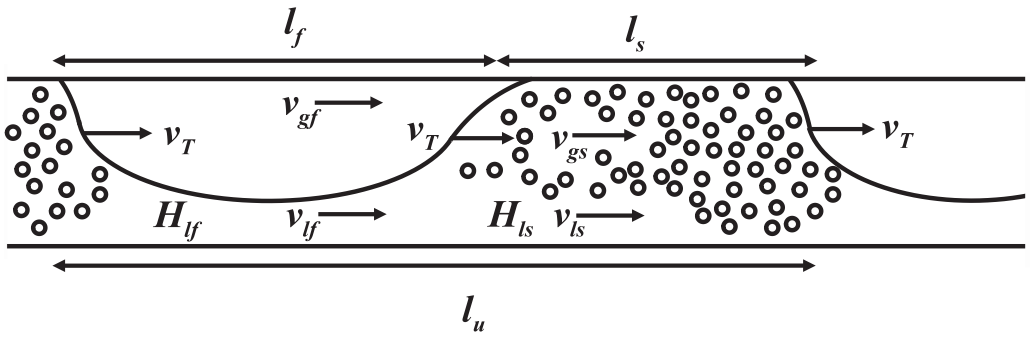

Fig. 3. Schematic representation of the unit slug in a pipe. (For horizontal piping, commonly: $v_{lf} < v_{ls} < v_{gs} < v_{gf} < v_T$.).

spikes of extremely short duration, i.e. microseconds to milliseconds) caused by slug impact on a solid wall.

Scaling rules will introduce errors so that safety margins in the design are required, and these may result in over-dimensioned piping structures. The conservatism in the bend-force estimation can be reduced by Computational Fluid Dynamics (CFD) simulations. Pontaza (2014), Pontaza et al. (2017) and Mack et al. (2018) presented accurate results of CFD calculations, but they also mentioned the extensive computational time required which limits the use of CFD in design and optimization. Hossain et al. (2019) used CFD to calculate flow quantities as liquid holdup, pressure, and average velocity, to solve a force balance over a pipe bend. Unlike Pontaza (2014), Hossain used a relatively coarse mesh and a simplified turbulence model, which reduced the computational time. Results were compared with the measured data from Liu et al. (2012). The RMS values of the momentum force contribution were well predicted, but the RMS value of the total force showed a different trend. Since the downstream piping of the measurement setup was not included in the simulation, the simulated pressures at the control volume differed from the measured pressures.

2. Mechanistic model

A stochastic mechanistic model is proposed to estimate the force of slug flow on pipe bends. The two-phase flow is represented by a train of slug units. The lengths of individual slug zones in the train are randomly selected from a probability distribution function. The fluctuating slug flow quantities (liquid holdup and fluid velocities) are then estimated with a slug model. Per zone, constant quantities are assumed. The liquid holdup H_l of a typical slug train is shown in Fig. 2, where the slug zone has a higher liquid holdup than the film zone. To calculate the force on the bend, time-varying quantities are substituted into the momentum balance of Eq. (4). The pressure at the control volume surfaces is calculated assuming a constant pressure at the pipe outflow.

Variations in velocity and liquid holdup between individual realizations of slug or film zones are much smaller than those between the zones themselves and therefore neglected; the force model assumes for simplicity that flow fluctuations can approximately be described by two alternating constant liquid holdup levels.

2.1. Unit slug model

New necessary adaptations to a unit slug model are proposed to include the stochastic character. A unit slug model is a simplified one-dimensional model describing slug flow as an aerated liquid zone and a film zone. The latter consists of a large bubble and a liquid film connected to the pipe wall. The model considers only one unit and consequently assumes that all slug units have the same length. Several unit slug models have been described in the literature, see Refs. Taitel and Barnea (1990), Gomez et al. (2000a), Zhang et al. (2003) and Smith et al. (2013). For its simplicity, the unit slug model of Gomez et al. (2000a) is used in this study. It consists of the continuity equation for both gas and liquid phases at cross-sections in the slug zone and in the film zone, a mass balance over the slug unit in the observer's reference frame and in a coordinate system moving with the constant translational velocity v_T, and the momentum balance in the film zone. Details can be found in Gomez et al. (2000a).

Fig. 3 shows schematically the unit slug. given superficial gas and liquid velocities u_g and u_l, densities ρ_g and ρ_l, viscosities, surface tension, wall roughness, and pipe diameter, one unique solution of the five balance equations exists. The liquid velocity in the slug v_{ls}, the film velocities of the gas and liquid v_{gf} and v_{lf}, the film liquid holdup H_{lf} and the fraction of the unit slug occupied by the slug zone l_s/l_u, are calculated. Herein is the unit slug length $l_u = l_s + l_f$, the sum of slug and film length. The system of equations needs to be completed with empirical or mechanistic sub-models for:

- The slug liquid holdup H_{ls}, which is estimated by the empirical correlation proposed by Gregory et al. (1978), noting that Gomez et al. (2000a) used the empirical correlation of Gomez et al. (2000b). Both Pereyra et al. (2012) and Al-Safran (2009) concluded that the empirical correlation of Gregory et al. (1978) outperformed other empirical slug liquid holdup relations published in the literature, including Gomez et al. (2000b).
- The gas–liquid interfaces velocity v_T, which differs from the slug zone velocities due to mass exchange between the zones. Eq. (5), the bubble velocity for two-phase flow in a pipe proposed by Nicklin et al. (1962b), is used. The drift velocity v_{drift} is modelled with the *Taylor* bubble correlation of Bendiksen (1984), which is

valid for bubbles with size of the same order of magnitude as the pipe diameter.

- The gas velocity in the slug v_{gs} is also calculated from Eq. (5), but the correlation of Harmathy (1960) for bubble sizes much smaller than the pipe diameter, is used. The correlation is valid for both vertical and horizontal flow.
- The pipe wall friction, estimated using the relation of Churchill (1977) which covers both the laminar and turbulent flow regimes. The wall friction of the liquid acts at the wetted part of the pipe and the friction of the gas acts at the dry part of the pipe. Additional roughness due to the presence of droplets and/or rivulets is not included. The Reynolds numbers used to calculate the friction factors are based on hydraulic diameters where only for the gas phase, the free interface width is included Gomez et al. (2000a).
- For the friction between gas and liquid in the stratified (flat) film, the 2008 version of the correlation proposed by Andritsos and Hanratty (1987), Andritsos et al. (2008) has been used, whereas Gomez et al. (2000a) used the 1987 version of the correlation (Andritsos and Hanratty, 1987).

The pressure gradient $(dp/dx)_f$ in the film zone is calculated from the local momentum balance and the pressure gradient $(dp/dx)_s$ in the slug zone is calculated using the homogeneous no-slip model. Deviating from the model of Gomez et al. (2000a), a *mixing pressure gradient* term is added to the slug pressure gradient to incorporate the liquid film acceleration when it merges into the faster flowing slug. The mixing pressure gradient $(dp/dx)_{mix}$, used by Kokal and Stanislav (1989) and Zhang et al. (2003) in their work, is essential to properly predict the pressure gradient in the slug. The force F_{lf} required to accelerate the liquid film is:

$$F_{lf} = \frac{dm}{dt}(v_{ls} - v_{lf}) . \tag{6}$$

where the liquid mass exchange flow rate $\frac{dm}{dt}$, flowing from film into slug, is:

$$\frac{dm}{dt} = \rho_l A H_f (v_T - v_{lf}) . \tag{7}$$

The momentum exchange at the slug-bubble interface will therefore introduce an additional pressure gradient for the entire unit slug:

$$(\frac{dp}{dx})_{mix} = \frac{\rho_l H_f (v_T - v_{lf})(v_{ls} - v_{lf})}{l_u} . \tag{8}$$

Both Kokal and Zhang assumed that the liquid in the film will completely be accelerated to the slug velocity v_{ls}. For shorter slugs, the liquid film will not accelerate completely before the liquid is released at the tail of the slug. A new mixture pressure drop correction for short slugs is proposed and used as an additional parameter in the model: when the slug zone is less than 0.2 of the unit length, the mixture pressure drop is scaled with the relative slug length l_s/l_u to incorporate the partly accelerated liquid film.

A pipe bend causes a pressure drop. This *minor loss* is estimated with a single-phase standard correlation (Idel'chik, 1996) for steady flow. The minor pressure gradient for the slug zone, $(dp/dx)_{bs}$, is calculated using slug mixture properties. The minor pressure gradient for the film zone, $(dp/dx)_{bf}$, is calculated using gas properties and the gas velocity in the film zone.

The model is valid for fully developed slug flow. The gas is modelled as an incompressible gas and consequently the model is only valid when the pressure drop is low, the gas density is approximately constant and phase changes can be neglected.

2.2. Stochastic slug model

The unit slug model predicts the constant fraction l_s/l_u and hence l_f/l_u but not one of the lengths l_u, l_s or l_f. In published slug models, constant lengths are assumed. In practice, the slug and film length vary, but this stochastic character does not follow from current theory. A new approach is proposed to include the stochastic character in the slug model by means of a statistical distribution. In the literature, both the inverse-Gaussian and the log-normal distribution have been proposed. Based on Al-Safran et al. (2008), the log-normal probability function is used herein:

$$P_{ln}(\xi) = \frac{1}{\xi\sqrt{2\pi\sigma}} \exp\left(-\frac{(\ln(\xi) - \mu)^2}{2\sigma^2}\right) \quad \xi > 0 . \tag{9}$$

where μ and σ are the mean and standard deviation of $\ln(l_s/D)$, the natural logarithm of the dimensionless slug length. The correlation for μ proposed by Al-Safran et al. (2008) has not been validated for high pressures and a different approach, based on slug frequency f_s defined as v_T/l_u, is used herein. Schulkes (2011) proposed a frequency correlation based on measurements including oil and gas under high pressure:

$$f_s = 0.016\frac{u_l}{D}\left(2 + 3\frac{u_l}{u_m}\right)\begin{cases} 12.1 Re_l^{-0.37} & Re_l < 4000 \\ 1 & Re_l \geq 4000 . \end{cases} \tag{10}$$

in which $Re_l = \rho_l u_l D/\mu_l$ is based on the liquid density ρ_l and dynamic viscosity μ_l. The slug length ratio l_s/l_u, calculated with the unit slug model, determines the mean slug zone length μ in the distribution:

$$\mu = \frac{v_T}{f_s D}\frac{l_s}{l_u} . \tag{11}$$

Utilizing a constant slug length ratio ensures mass conservation when the stochastics is introduced into the slug model. For σ, the expression proposed by Al-Safran et al. (2008) is used:

$$\sigma = 0.298 - 1.027 H_f + 0.995\frac{H_f(u_m - v_{lf})(v_T - v_{lf})}{u_m^2} . \tag{12}$$

Individual slug lengths $\tilde{l_s}$ are calculated by randomly selecting lengths according to the distribution Eq. (9). The corresponding film length $\tilde{l_f}$ is calculated from the predicted slug length fraction l_s/l_u. Typical slug and film length histograms are shown in Fig. 4.

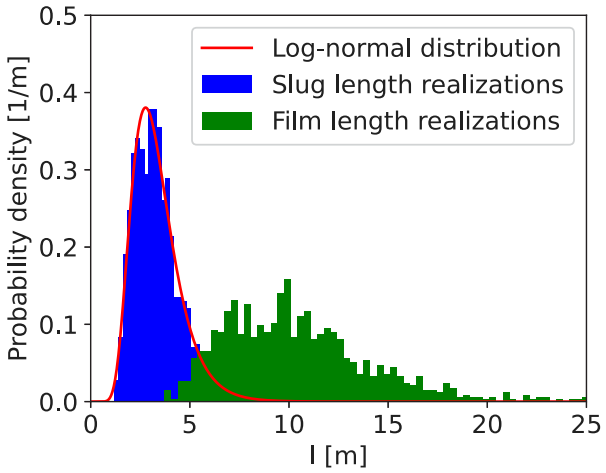

Fig. 4. Example of calculated slug and film length probability distribution, $D = 0.07$ m, $\mu = 3.35$, $\sigma = 0.35$ and $l_s/l_u = 0.24$.

2.3. Pressure variations

The pressure gradient in steady slug flow is a function of time and distance. The surface integral of the pressure part in Eq. (4) is:

$$\int_{CS} p d\mathbf{A} = A\begin{pmatrix} p_{in} \\ p_{out} \end{pmatrix} . \tag{13}$$

The pressures p_{in} and p_{out} at the bend inlet and outlet are calculated on the basis of a constant outflow pressure p_o at a distance l_{ds} downstream

Fig. 5. Example of the slug length and film length in piping downstream of the bend.

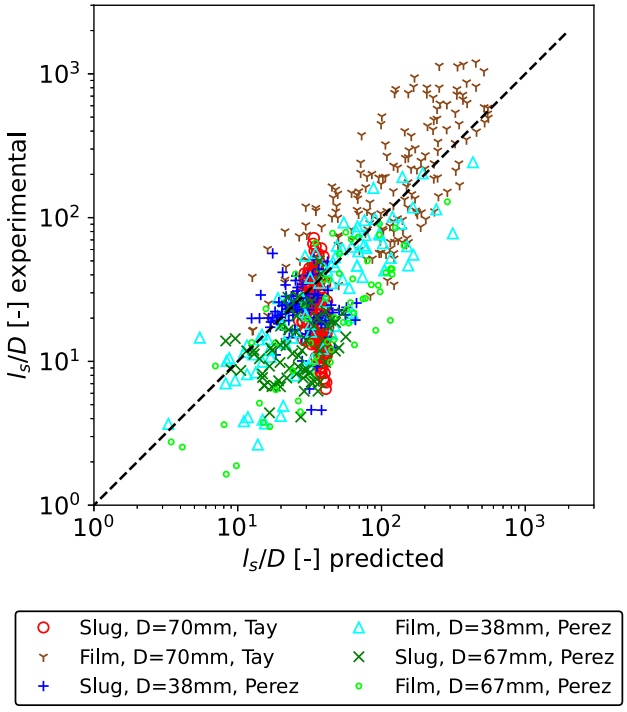

Fig. 6. Predicted average slug and film lengths by Eq. (11) compared with measurements.

of the bend. This assumption reflects the outflow condition in most of the experimental setups used to validate the model. Because the pressure gradient in the slug zone differs from that in the film zone, the pressure at an arbitrary location A along the pipe depends on the sum of the slug lengths and the sum of the film lengths in-between location A and the outflow. These lengths are changing in time, which causes a fluctuating pressure at location A, see Fig. 5. When the pressure gradients for the slug and the film zones are known, the pressure at location A can be estimated by calculating the length fractions λ_s^A and λ_f^A of the downstream piping occupied by slug zones and film zones, respectively.

The *minor loss* caused by the bend comes in addition to the frictional pressure loss and is a result of flow separation downstream of the bend. Sanchez Silva et al. (2010) observed that for two-phase flow the main part of the minor loss spreads over a fixed length of $L \sim 30D$ downstream of the bend, affecting the pressure at the bend control volume boundaries. This is about the same length as measured by Itō (1960) for single-phase flow and used by Tay and Thorpe (2014) in their model. As with the frictional losses, the minor loss is estimated by calculating the slug and film length fractions λ_s^b and λ_f^b in the $30D$ pipe section downstream of the bend. The minor losses are equally divided over this length.

When the bend outlet is chosen as location A, the downstream piping has a length of l_{ds} and the pressure p_{out} is:

$$p_{out}(t) = p_0 + l_{ds}\left[\lambda_s^{out}(t)\left(\frac{dp}{dx}\right)_s + \lambda_s^{out}(t)\left(\frac{dp}{dx}\right)_f\right] + 30D\left[\lambda_s^b(t)\left(\frac{dp}{dx}\right)_{bs} + \lambda_f^b(t)\left(\frac{dp}{dx}\right)_{bf}\right], \tag{14}$$

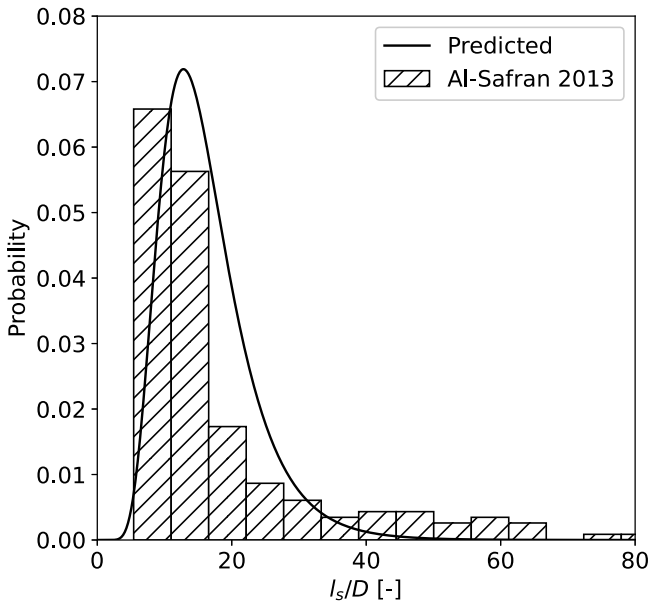

Fig. 7. Predicted slug length distribution compared with measurements from Al-Safran et al. (2013).

where the superscript *out* replaces A and the superscript b stands for bend. When the bend inlet is chosen as location A and the bend's radius of curvature is R, the downstream piping has a length of $\frac{\pi}{2}R + l_{ds}$ and the length fractions, with superscript A replaced by *in*, differ from the ones used in Eq. (14). The pressure p_{in} is:

$$p_{in}(t) = p_0 + \left(l_{ds} + \frac{\pi}{2}R\right)\left[\lambda_s^{in}(t)\left(\frac{dp}{dx}\right)_s + \lambda_f^{in}(t)\left(\frac{dp}{dx}\right)_f\right] + 30D\left[\lambda_s^b(t)\left(\frac{dp}{dx}\right)_{bs} + \lambda_f^b(t)\left(\frac{dp}{dx}\right)_{bf}\right]. \tag{15}$$

2.4. Momentum terms

The second surface integral in Eq. (4) describes the momentum flowing in and out of the control volume shown in Fig. 1:

$$-\int_{CS} \mathbf{v}\rho(\mathbf{v}\cdot\mathbf{n})\,dA = -A\begin{pmatrix}\rho v^2\\ \rho v^2\end{pmatrix}, \tag{16}$$

where v is specified later. When the slug front passes location A in Fig. 5, the instantaneous liquid and gas mass flow is:

$$\begin{aligned}\dot{m}_l &= v_T A H_{ls}\rho_l\,,\\ \dot{m}_g &= v_T A(1-H_{ls})\rho_g\,.\end{aligned} \tag{17}$$

Due to the gradual inflow of liquid from the film, the mass flow decreases towards the tail of the slug. Following the model concept of constant quantities per zone, the slug zone mass flows according to Eq. (17) are assumed. For the liquid and gas mass flow in the film zone, the slug liquid holdup H_{ls} in Eq. (17) is replaced with the film liquid holdup H_{lf}. The gas and liquid velocities as shown in Fig. 3 are used to calculate the momentum surface integral in Eq. (4):

$$-\int_{CS,s} \mathbf{v}\rho(\mathbf{v}\cdot\mathbf{n})dA = \left(v_{ls}v_T A H_{ls}\rho_l + v_{gs}v_T A(1-H_{ls})\rho_g\right)\begin{pmatrix}1\\1\end{pmatrix} \tag{18a}$$

$$-\int_{CS,f} \mathbf{v}\rho(\mathbf{v}\cdot\mathbf{n})dA = \left(v_{lf}v_T A H_{lf}\rho_l + v_{gf}v_T A(1-H_{lf})\rho_g\right)\begin{pmatrix}1\\1\end{pmatrix}, \tag{18b}$$

where the first (slug) or second (film) equation is used, depending on which zone flows through the control volume boundary.

The volume integral in Eq. (4) describes the change in time of momentum M inside the control volume shown in Fig. 1, which is only

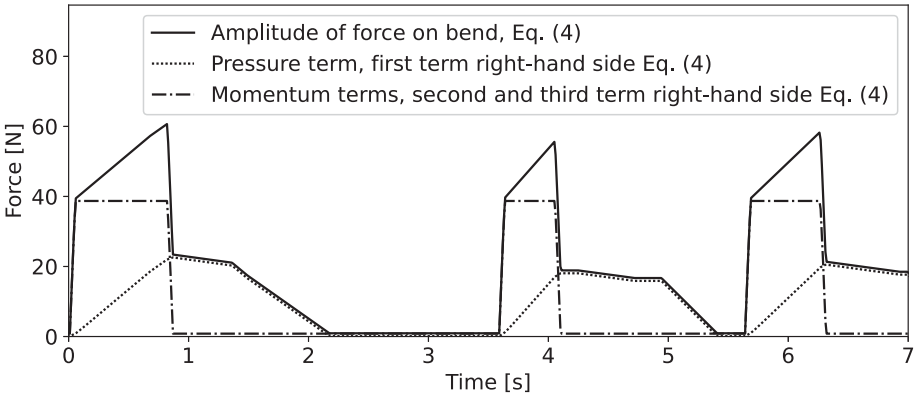

Fig. 8. Total force amplitude and a split into pressure and momentum contribution, for air–water slug flow, $u_l = 0.5$ m/s, $u_g = 2$ m/s, $D = 70$ mm, bend radius $R = 1.5D$ and pipe wall roughness of 0.01 mm.

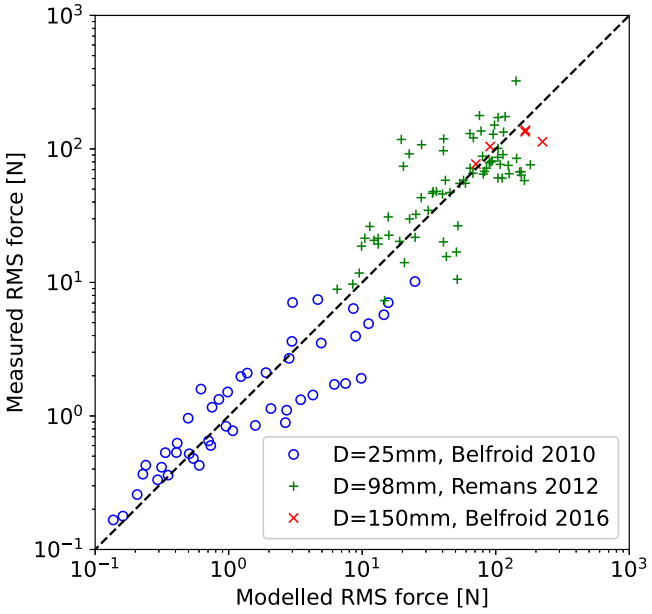

Fig. 9. Measured and modelled RMS force on pipe bends.

non-zero when the slug front or the slug tail is inside the bend:

$$-\frac{d}{dt}\int_{CV}\mathbf{v}\rho dV = \begin{pmatrix} M_x \\ M_y \end{pmatrix}. \tag{19}$$

M_x and M_y are derived below. When the bend is completely filled with either a slug or a film zone, the momentum within the bend is constant and the time derivative is zero. This integral is calculated for the (unlikely) situation where both slug front and slug tail are inside the control volume. For situations where only the slug front or tail is inside the bend, the momentum change can be obtained by removing the upstream or the downstream film term out of Eqs. (20) and (21).

$$\begin{aligned} M_x(t) = Av_T \Big[& \left(u_{lf}\rho_l H_{lf} + u_{gf}\rho_g(1-H_{lf})\right) \\ & \times \left(\cos(\frac{v_T t}{R}) - \cos(\frac{v_T t - l_s}{R})\right) + \\ & \left(u_{ls}\rho_l H_{ls} + u_{gs}\rho_g(1-H_{ls})\right)\left(\cos(\frac{v_T t - l_s}{R}) - \cos(\frac{v_T t}{R})\right)\Big] \end{aligned} \tag{20}$$

$$\begin{aligned} M_y(t) = Av_T \Big[& \left(u_{lf}\rho_l H_{lf} + u_{gf}\rho_g(1-H_{lf})\right) \\ & \times \left(\sin(\frac{v_T t - l_s}{R}) - \sin(\frac{v_T t}{R})\right) + \\ & \left(u_{ls}\rho_l H_{ls} + u_{gs}\rho_g(1-H_{ls})\right)\left(\sin(\frac{v_T t}{R}) - \sin(\frac{v_T t - l_s}{R})\right)\Big] \end{aligned} \tag{21}$$

2.5. Solution method

The gas and the liquid velocities, the liquid holdup, the pressure gradient and the slug length fraction l_s/l_u are calculated for both slug and film zone. A liquid holdup time-signal with the two discrete holdup levels H_{ls} and H_{lf} is defined (Fig. 2), where the length l_s is randomly selected according the log-normal distribution defined by Eq. (9). The length $l_f = l_u - l_s$ is calculated using the slug length fraction l_s/l_u. A Lagrangian tracking method, calculating the location of all the slug–film interfaces, is used to calculate the force on the bend from algebraic Eqs. (14), (15), (18a), (18b), (20) and (21).

3. Results

In Fig. 6, average slug and film length predictions are compared with measured values published by Tay and Thorpe (2004) and Perez (2008). Shorts slugs are over-predicted and this error will propagate in the force predictions. Bubble lengths are well predicted.

Slug-length probability results are compared with slug lengths measured by Al-Safran et al. (2013) in Fig. 7.

The proposed solution method is used to solve Eq. (4) for a water–air slug flow through a horizontal pipe bend ($u_l = 0.5$ m/s, $u_g = 2$ m/s, $D = 70$ mm and $R = 1.5D$). The pipe length downstream of the bend is $65D$ and the first two slugs are $40D$ and $22D$ long. The length of F_{bend} and the contribution of pressure and momentum to this force, are shown in Fig. 8.

Initially, the bend and its downstream leg is filled with a film zone. The momentum flowing in and out of the control volume (Eq. (18b)) is close to zero and the pressure in the bend is approximately atmospheric. At $t = 0.0$ s, the slug front arrives at the bend and the momentum change increases rapidly (Eq. (18a)). As a result of liquid flowing into the downstream piping and its friction, the pressure in the bend increases. At $t = 0.8$ s, the slug leaves the bend, the momentum change decreases rapidly and the maximum bend pressure is reached since the complete slug is downstream of the bend. The small pressure decrease in between $t = 0.8$ s and $t = 1.4$ s is caused by the slug flowing out of the $30D$ zone where the bend minor losses are dissipated. At

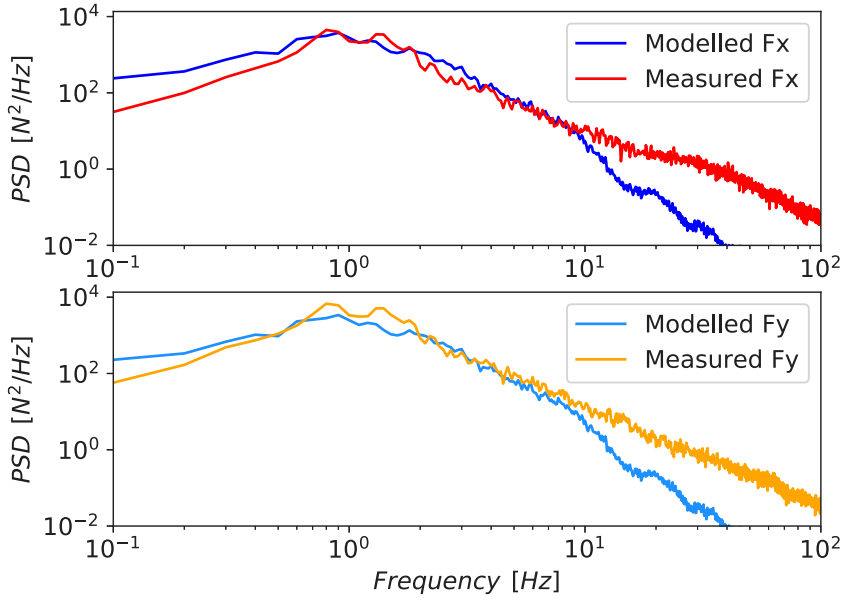

Fig. 10. Force spectrum of slug flow in $D = 150$ mm pipe with long slugs.

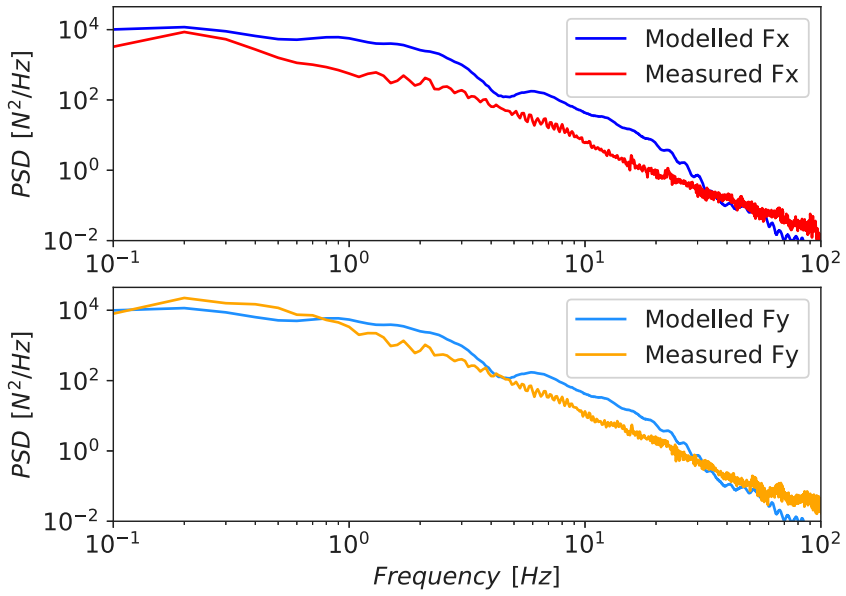

Fig. 11. Force spectrum of slug flow in $D = 150$ mm pipe with short slugs.

$t = 1.4$ s, the slug front has reached the outflow and the bend pressure decreases up to the instant that the complete slug is out of the pipe. At $t = 4.3$ s, a second slug arrives at the bend. This slug is shorter (because of the stochastics) which results in a lower bend pressure when the complete slug is in the downstream piping. The amplitude of momentum change is independent of slug length.

The calculated forces, using the stochastic distribution of Eq. (9) with predicted $\ln(l_s/D)$ mean and standard deviation (Eqs. (11) and (12)) as closure in the slug model, are compared with published measurements. Details of the laboratory setups and the tests are shown in Table 1. Belfroid et al. (2010, 2016) and Remands et al. (2012) reported the Root Mean Square (RMS) value and the Power Spectral Density (PSD) of the force, measured on a pipe bend. The supports used for the 25 mm and 98 mm diameter piping did allow for undesired pipe movements introducing some error. The supports of the 150 mm diameter laboratory setup (Belfroid et al., 2018) were stiff and the pipe did not vibrate at frequencies below 40 Hz. The length of the piping downstream of the bend is estimated from the laboratory setup figures shown in the papers. Air and water were used in Belfroid's and Remans experiments. Tay and Thorpe (2004) published the measured peak value of the force on a pipe bend with stiff supports. Bellows were used to uncouple the bend from pipe movements. Tay and Thorpe (2004) used air and water, IPA (5 wt%), or glycerol (35 wt%) solutions in their experiments.

Table 1
Pipe size, bend radius and flow velocities in published measurements.

Source	D [mm]	R/D [–]	Superficial velocities [m/s]	
			Gas	*Liquid*
Belfroid et al. (2010)	25	0.5	0.2–9.1	0.2–1.0
Tay and Thorpe (2004)	70	0.5	0.4–2.9	0.2–0.7
Remands et al. (2012)	98	1.5	0.4–8.0	0.1–2.9
Belfroid et al. (2018)	150	1.5	0.9–10.4	0.5–2.0

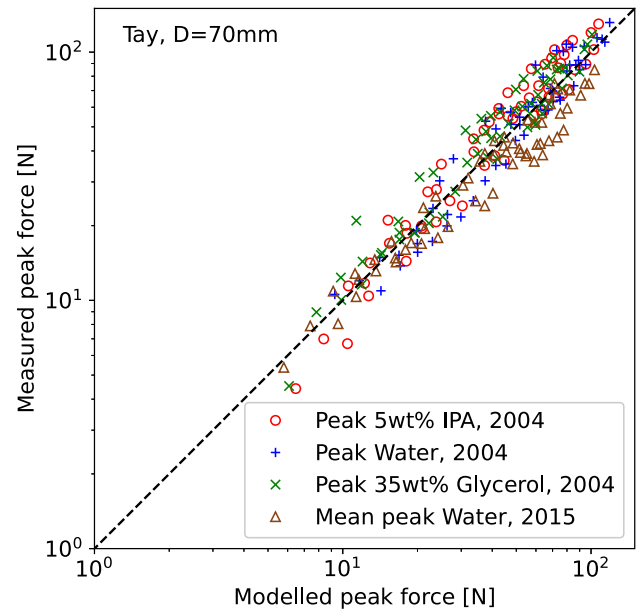

Fig. 12. Peak value of the force on a bend.

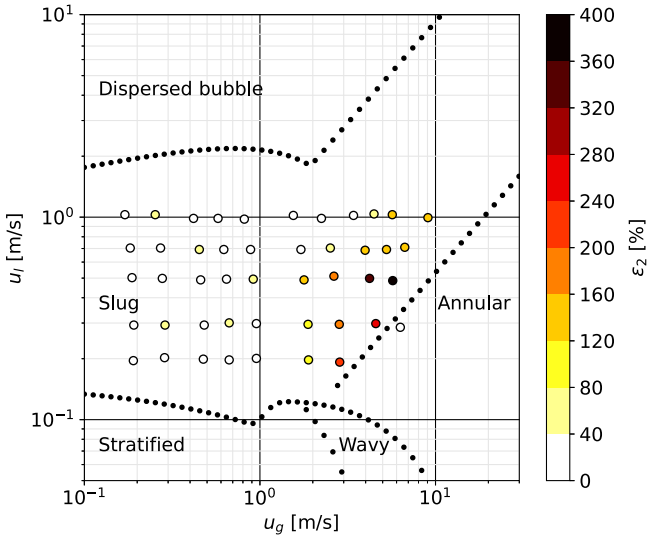

Fig. 13. Relative error of the RMS force for 25 mm pipe (Belfroid et al., 2010) shown in the flow regime map of Gomez et al. (2000a).

In Fig. 9, the RMS values of the modelled bend force are compared with the measured values. An absolute pressure of 1 atmosphere is assumed at the pipe outflow.

The correlation Eq (3) proposed by Belfroid et al. (2018) is developed from the same data as used in Fig. 9. A comparison of the correlation with measurements can be found in Belfroid et al. (2018). In some cases, where a slug was observed in the measurements, the governing equations predicted a negative film or slug zone length, indicating the boundaries of our model; usually a transition to another flow regime takes place. Zhang et al. (2003) used this slug model feature to predict flow regime borders, bubbly flow for zero or negative film-zone lengths, and a separated regime (stratified or annular) for zero or negative slug length. The modelled and measured force spectra of two cases are shown in Figs. 10 and 11.

In Fig. 12, the model results of the peak force are compared with the measurements published by Tay and Thorpe (2004, 2017).

Table 2
Error statistics.

	ϵ_{r1} [%]	ϵ_{r2} [%]	σ_{r2} [%]	ϵ_{a1} [N]	ϵ_{a2} [N]	σ_{a2} [N]
RMS	28	62	92	5	27	61
Peak	1.4	17	22	−1.4	8.2	11

Statistical parameters are used to quantify the difference between modelled and measured RMS forces. The definitions can be found in the Appendix. The measurement error itself could not be estimated from the publications. Results of the statical evaluation of the RMS and peak force predictions are shown in Table 2. As illustrated in Fig. 13, the larger errors were found for slug flow cases close to the annular flow regime. For those cases, the flow could have been in a mixed slug-annular transition regime where the assumption of two discrete (film and slug) states is not valid.

4. Conclusions

An existing slug-force-on-bend model, where a fixed slug propagation velocity was assumed as model input together with the measured average slug length, has been improved. In the new model, the slug and film zone velocities are obtained from a mechanistic unit-slug model. The predicted force fluctuations are caused by density, pressure, and velocity variations. A log-normal slug length distribution is used to introduce the stochastics in the fluctuation when alternating slug and film zones pass the bend.

The proposed stochastic mechanistic model is able to predict the force of hydrodynamic slug flow through a pipe bend. The prediction trend is good for all tested pipe diameters and fluid properties, except for flow cases in the slug-annular transition region. In contrast to the discrete power spectrum obtained for mean slug-length-based models, which have periodic excitation of the bend, the power spectra of the stochastic mechanistic model are continuous and in line with the observations.

The model encompasses the conservation of mass and momentum and can be used outside of the measurement range used for the validation herein. The calculation time on a single 3 GHz processor is less than 20 seconds, which means a speed-up factor of 10^5 compared to CFD calculations.

CRediT authorship contribution statement

Arnout M. Klinkenberg: Conceived of the presented idea, developed the theory, collected the data, performed the computations, wrote the draft manuscript, discussed the results, contributed to the final manuscript. **Arris S. Tijsseling:** Provided critical feedback, verified the analytical method, supervised the findings of this work, helped to shape the final manuscript, discussed the results, contributed to the final manuscript.

Declaration of competing interest

The authors declare that they have no known competing financial interests or personal relationships that could have appeared to influence the work reported in this paper.

Acknowledgment

This research did not receive any specific grant from funding agencies in the public, commercial, or not-for-profit sectors.

Appendix. Error definitions

The statistical parameters are calculated from the relative and actual errors e_r and e_a:

$$e_r = \frac{F_{cal} - F_{exp}}{F_{exp}} 100\% , \tag{A.1}$$

and

$$e_a = F_{cal} - F_{exp} , \tag{A.2}$$

where F is the RMS or amplitude peak value of the bend force and the subscripts *cal* and *exp* are the calculated and experimental values, respectively. The average relative and actual error ϵ_{r1} and ϵ_{a1} are:

$$\epsilon_{r1} = \frac{1}{N} \sum_{i=1}^{N} e_{r,i} , \tag{A.3}$$

and

$$\epsilon_{a1} = \frac{1}{N} \sum_{i=1}^{N} e_{a,i} , \tag{A.4}$$

where N is the number of unique (i.e. no repetition) measurements used in the statistical evaluation. To prevent average error distortion due to cancellation of positive and negative error values, the errors based on the absolute values are calculated:

$$\epsilon_{r2} = \frac{1}{N} \sum_{i=1}^{N} |e_{r,i}| \tag{A.5}$$

and

$$\epsilon_{a2} = \frac{1}{N} \sum_{i=1}^{N} |e_{a,i}| . \tag{A.6}$$

The scattering of the errors is quantified by the standard deviation of the absolute average errors:

$$\sigma_{r2} = \sqrt{\frac{1}{N-1} \sum_{i=1}^{N} (e_{r,i} - \epsilon_{r2})^2} , \tag{A.7}$$

and

$$\sigma_{a2} = \sqrt{\frac{1}{N-1} \sum_{i=1}^{N} (e_{a,i} - \epsilon_{a2})^2} . \tag{A.8}$$

References

Al-Safran, E., 2009. Prediction of slug liquid holdup in horizontal pipes. J. Energy Resour. Technol. 131 (2), http://dx.doi.org/10.1115/1.3120305.

Al-Safran, E., Gokcal, B., Sarica, C., et al., 2013. Investigation and prediction of high-viscosity liquid effect on two-phase slug length in horizontal pipelines. SPE Prod. Oper. 28 (03), 296–305. http://dx.doi.org/10.2118/150572-PA.

Al-Safran, E., Sarica, C., Zhang, H., Brill, J., 2008. Probabilistic mechanistic modeling of slug length distribution in a horizontal pipeline. SPE Prod. Facil. 20 (2), 160–172. http://dx.doi.org/10.2118/84230-PA.

Andritsos, N., Hanratty, T., 1987. Influence of interfacial waves in stratified gas-liquid flows. AIChE J. 33 (3), 444–454. http://dx.doi.org/10.1002/aic.690330310.

Andritsos, N., Tzotzi, C., Hanratty, T., 2008. Interfacial shear stress in wavy stratified gas liquid two phase flow. In: 5th European Thermal-Sciences Conference EUROTHERM, Eindhoven, the Netherlands.

Belfroid, S., Nennie, E., Lewis, M., 2016. Multiphase forces on bends - large scale 6-inch experiments. In: SPE Annual Technical Conference and Exhibition. UAE, Dubai.

Belfroid, S., Nennie, E., Lewis, M., 2018. Influence bend radius on multiphase flow induced forces on a bend structure. In: Proceedings of the 9th International Symposium on Fluid-Structure Interactions, Flow-Sound Interactions, Flow-Induced Vibration and Noise, Toronto, Canada.

Belfroid, S., Schiferli, W., Cargnelutti, M., van Osch, M., 2010. Forces on bends and T-joints due to multiphase flow. ASME 2010 3rd Joint US-European Fluids Engineering Summer Meeting Collocated with 8th International Conference on Nanochannels, Microchannels, and Minichannels, Montreal, Canada 613–619.

Bendiksen, K.H., 1984. An experimental investigation of the motion of long bubbles in inclined tubes. Int. J. Multiph. Flow. 10 (4), 467–483. http://dx.doi.org/10.1016/0301-9322(84)90057-0.

Churchill, S.W., 1977. Friction-factor equation spans all fluid-flow regimes. Chem. Eng. 84 (24), 91–92.

Giraudeau, M., Mureithi, N., Pettigrew, M., 2013. Two-phase flow-induced forces on piping in vertical upward flow: Excitation mechanisms and correlation models. J. Press. Vessel Technol. 135, 030907–030907–16.

Giraudeau, M., Pettigrew, M., Mureithi, N., 2011. Two-phase flow excitation forces on a vertical u-bend tube. In: Proceedings of the ASME 2011 Pressure Vessel and Piping Division Conference, Vol. 4. pp. 103–111. http://dx.doi.org/10.1115/PVP2011-57103.

Gomez, L., Shoham, O., Schmidt, Z., Chokshi, R., Northug, T., 2000a. Unified mechanistic model for steady-state two-phase flow: horizontal to vertical upward flow. SPE J. 5 (03), 339–350. http://dx.doi.org/10.2118/65705-PA.

Gomez, L., Shoham, O., Taitel, Y., 2000b. Prediction of slug liquid holdup: horizontal to upward vertical flow. Int. J. Multiph. Flow. 26 (3), 517–521. http://dx.doi.org/10.1016/S0301-9322(99)00025-7.

Gregory, G., Nicholson, M., Aziz, K., 1978. Correlation of the liquid volume fraction in the slug for horizontal gas-liquid slug flow. Int. J. Multiph. Flow. 4 (1), 33–39. http://dx.doi.org/10.1016/0301-9322(78)90023-X.

Harmathy, T.Z., 1960. Velocity of large drops and bubbles in media of infinite or restricted extent. AIChe J. 6 (2), 281–288. http://dx.doi.org/10.1002/aic.690060222.

Hossain, M., Chinenye-Kanu, N.M., Droubi, G.M., Islam, S.Z., 2019. Investigation of slug-churn flow induced transient excitation forces at pipe bend. J. Fluids Struct. 91, 102733. http://dx.doi.org/10.1016/j.jfluidstructs.2019.102704.

Idel'chik, I., 1996. Handbook of Hydraulic Resistance, third ed..

Itō, H., 1960. Pressure losses in smooth pipe bends. J. Basic Eng. 82, 131–140. http://dx.doi.org/10.2495/CMEM-V6-N1-198-207.

Kokal, S., Stanislav, J., 1989. An experimental study of two-phase flow in slightly inclined pipes—I. flow patterns. Chem. Eng. Sci. 44 (3), 665–679. http://dx.doi.org/10.1016/0009-2509(89)85042-0.

Liu, Y., Miwa, S., Hibiki, T., Ishii, M., Morita, H., Kondoh, Y., Tanimoto, K., 2012. Experimental study of internal two-phase flow induced fluctuating force on a 90° elbow. Chem. Eng. Sci. 76, 173–187. http://dx.doi.org/10.1016/j.ces.2012.04.021.

Mack, A., Joshi, H., Belfroid, S., 2018. Numerical rebuilding of dynamic instabilities and forces in multiphase pipe bend flow. Int. J. Comput. Methods Exp. Meas. 6 (2), 358–372. http://dx.doi.org/10.2495/CMEM-V6-N2-358-372.

Miwa, S., Mori, M., Hibiki, T., 2015. Two-phase flow induced vibration in piping systems. Prog. Nucl. Energy 78, 270–284. http://dx.doi.org/10.1016/j.pnucene.2014.10.003.

Nennie, E., Belfroid, S., O'Mahoney, T., 2013. Validation of CFD and simplified models with experimental data for multiphase fluid structure interaction with multiple bends. 8th International Conference of Multiphase Flow ICMF 2013, Jeju, Korea..

Nicklin, D., Wilkens, J., Davidson, J., 1962a. Two-phase flow in vertical pipes. Trans. Chem. Inst. Chem. Eng. 40, 61–68.

Nicklin, D., Wilkes, M., Davidson, M., 1962b. Two-phase flow in vertical tubes. Chem. Eng. Sci. 17 (61), 61–68.

Pereyra, E., Arismendi, R., Gomez, L.E., Mohan, R.S., Shoham, O., Kouba, G.E., 2012. State of the art of experimental studies and predictive methods for slug liquid holdup. J. Energy Resour. Technol. 134 (2), http://dx.doi.org/10.1115/1.4005658.

Perez, V.H., 2008. Gas-Liquid Two-Phase Flow in Inclined Pipes (Ph.D. thesis).

Pontaza, J., 2014. Fluid structure interaction and screening pipeline span VIV and subsea piping FIV. In: Offshore Technology Conference. Houston, USA, http://dx.doi.org/10.4043/25429-MS.

Pontaza, J.P., Menon, R.G., 2011. Flow-induced vibrations of subsea jumpers due to internal multi-phase flow. In: ASME 2011 30th International Conference on Ocean. Offshore and Arctic Engineering, Rotterdam, the Netherlands, http://dx.doi.org/10.1115/OMAE2011-50062.

Pontaza, J., Smith, F., Bezensek, B., Ho, C., 2017. Adoption of the flow induced vibration FIV intermediate screening methodology on the OLLLR project. In: Underwater Technology Conference, Bergen, Norway.

Remands, D., van Bokhorst, E., Nennie, E., Belfroid, S., 2012. Multiphase fluid structure interaction in pipe systems with multiple bends. In: FIV2012, 10th International Conference on Flow-Induced Vibration (& Flow-Induced Noise), Dublin, Ireland.

Riverin, J., de Langre, E., Pettigrew, M., 2006. Fluctuating forces caused by internal two-phase flow on bends and tees. J. Sound Vib. 298 (4-5), 1088–1098. http://dx.doi.org/10.1016/j.jsv.2006.06.039.

Riverin, J., Pettigrew, M., 2007. Vibration excitation forces due to two-phase forces in piping elements. J. Press. Vessel Technol. 192, 7–13. http://dx.doi.org/10.1115/1.2388994.

Sanchez Silva, F., Luna Resendiz, J., Carvajal Mariscal, I., Tolentino Eslava, R., 2010. Pressure drop models evaluation for two-phase flow in 90 degree horizontal elbows. Ing. Mec. Tecnol. Des. 3 (4), 115–122.

Schulkes, S., 2011. Slug frequencies revisited. In: 15th International Conference on Multiphase Production Technology, Cannes, France.

Smith, I.E., Nossen, J., Undander, T.E., 2013. Improved holdup and pressure drop predictions for multiphase flow with gas and high viscosity oil. In: 16th International Conference on Multiphase Production Technology, Cannes, France.

Taitel, Y., Barnea, D., 1990. Two-phase slug flow. Adv. Heat Transf. 20, 83–132. http://dx.doi.org/10.2118/98-39.

Tay, B., Thorpe, R., 2004. Effects of liquid physical properties on the forces acting on a pipe bend in gas–liquid slug flow. Chem. Eng. Res. Des. 82 (3), 344–356. http://dx.doi.org/10.1205/026387604322870453.

Tay, B., Thorpe, R., 2014. Hydrodynamic forces acting on pipe bends in gas-liquid slug flow. Chem. Eng. Res. Des. 92 (5), 812–825. http://dx.doi.org/10.1016/j.cherd.2013.08.012.

Tay, B., Thorpe, R., 2017. Statistical analysis of the hydrodynamic forces acting on pipe bends in gas–liquid slug flow and their relation to fatigue. Chem. Eng. Res. Des. 104, 457–471. http://dx.doi.org/10.1016/j.cherd.2015.07.028.

Urthaler, Y., Breaux, L.E., McNeill, S.I., Luther, E.M., Austin, J., Tognarelli, M., 2011. A methodology for assessment of internal flow-induced vibration (FIV) in subsea piping systems. In: ASME 2011 30th International Conference on Ocean. Offshore and Arctic Engineering, Rotterdam, the Netherlands, http://dx.doi.org/10.1115/OMAE2011-49795.

Yih, T., Griffith, P., 1968. Unsteady Momentum Fluxes in Two-Phase Flow and the Vibrations of Nuclear Reactor Components. Report No. DSR 70318-58, Department of Mechanical Engineering, Massachusetts Institute of Technology.

Zhang, H.-Q., Wang, Q., Sarica, C., Brill, J.P., 2003. A unified mechanistic model for slug liquid holdup and transition between slug and dispersed bubble flows. Int. J. Multiph. Flow. 29 (01), 97–107. http://dx.doi.org/10.1016/S0301-9322(02)00111-8.

Zukoski, E.E., 1966. Influence of viscosity, surface tension, and inclination angle on motion of long bubbles in closed tubes. J. Fluid Mech. 25, 821–837.